

Are Particles in Advection–Dominated Accretion Flows Thermal?

Rohan Mahadevan¹ and Eliot Quataert²

Harvard-Smithsonian Center for Astrophysics, 60 Garden St., Cambridge, MA 02138

ABSTRACT

We investigate the form of the momentum distribution function for protons and electrons in an advection–dominated accretion flow (ADAF). We show that for all accretion rates, Coulomb collisions are too inefficient to thermalize the protons. The proton distribution function is therefore determined by the viscous heating mechanism, which is unknown. The electrons, however, can exchange energy quite efficiently through Coulomb collisions and the emission and absorption of synchrotron photons. We find that for accretion rates greater than $\sim 10^{-3}$ of the Eddington accretion rate, the electrons have a thermal distribution throughout the accretion flow.

For lower accretion rates, the electron distribution function is determined by the electron’s source of heating, which is primarily adiabatic compression. Using the principle of adiabatic invariance, we show that an adiabatically compressed collisionless gas maintains a thermal distribution until the particle energies become relativistic. We derive a new, non–thermal, distribution function which arises for relativistic energies and provide analytic formulae for the synchrotron radiation from this distribution. Finally, we discuss its implications for the emission spectra from ADAFs.

Subject headings: accretion, accretion disks — black hole physics — radiation mechanisms: thermal, non–thermal — galaxies: elliptical and lenticular, cD — radio continuum: galaxies — Galaxy: general

1. Introduction

An advection–dominated accretion flow is a hot, optically thin, accretion flow with low radiative efficiency (Abramowicz et al. 1988; Narayan & Yi 1994, 1995a, 1995b; Abramowicz et al. 1995). Unlike standard thin disks (see Frank et al. 1992), where all

¹rmahadevan@cfa.harvard.edu

²equataert@cfa.harvard.edu

of the viscously generated energy is thermalized and radiated locally, ADAFs store most of the viscously generated energy as internal energy of the ions and advect it onto the central object. The gas in an ADAF is a two temperature plasma, with the ions being significantly hotter than the electrons (Shapiro et al. 1976; Rees et al. 1982). Since most of the viscously generated energy is assumed to heat the ions, and only a small fraction of this energy is transferred to the electrons via Coulomb collisions, the total energy radiated is much less than the total energy generated by viscosity (Rees et al. 1982).

The emission spectrum from an ADAF is determined by the cooling mechanisms of the protons and electrons. The protons cool very inefficiently, primarily through proton–proton collisions which create neutral pions. The pions decay into γ –rays with mean frequencies $\sim 10^{24}$ Hz (Mahadevan et al. 1997). The electrons, on the other hand, cool very efficiently through synchrotron, bremsstrahlung, and Compton processes. Detailed calculations of these cooling mechanisms lead to ADAF models which have been successfully applied to explain the observed radio to gamma-ray spectrum from a number of accreting black hole systems. These include solar mass black holes in X-ray binaries, e.g., A0620 and V404Cyg (Narayan, McClintock, & Yi 1996), as well as supermassive black holes at the centers of galaxies, e.g., Sgr A* (Narayan et al. 1995; Mahadevan et al. 1997) and NGC 4258 (Lasota et al. 1996).

The shape and magnitude of an ADAF spectrum depends primarily on the mass accretion rate and, to a lesser extent, on the mass of the accreting object (Narayan & Yi 1995b; Narayan 1996). In determining the spectrum, however, all previous work has assumed that the electrons are thermal throughout the ADAF. This is a crucial assumption, since the emergent spectrum would be considerably different for different electron distribution functions. In the present paper, we investigate the validity of this assumption.

We treat thermalization within the ADAF paradigm. We assume that the only physical interactions among particles are Coulomb collisions and self–absorbed synchrotron radiation. We do not consider the possible non–thermal heating of electrons by wave–particle interactions, magnetic reconnection, or collective plasma effects. The interactions considered here therefore incorporate only the well understood physical processes in ADAFs.

The outline of the paper is as follows. In the following section (§2) we present the necessary background equations and consider proton thermalization by Coulomb collisions. In §3 we investigate the form of the electron distribution function, in particular for suprathermal electron energies, and determine the mass accretion rates for which electrons are thermalized by Coulomb collisions or self–absorbed synchrotron radiation. In §4 we consider the form of the electron distribution function when thermalization is inefficient, which depends on the interplay between the heating and cooling mechanisms. We give a new (non-thermal) distribution function, valid when the electrons compress

adiabatically to relativistic energies. In §5 we give the synchrotron spectrum from this new distribution function and in §6 we discuss the implications and possible applications of our results.

2. General Relations

2.1. Self-similar Flow Equations

The parameters which determine the structure of an ADAF are the viscosity parameter, α (Shakura & Sunyaev 1973), the ratio of the gas pressure to the total pressure, β_{adv} , the mass of the central object, $M = m M_{\odot}$, where m is the mass in solar mass units, and the accretion rate, $\dot{M} = \dot{m} \dot{M}_{\text{Edd}}$, where \dot{m} is the accretion rate in Eddington units ($\dot{M}_{\text{Edd}} = 1.39 \times 10^{18} m \text{ g s}^{-1}$). Typical values for α and β_{adv} which have been successfully applied to observed systems are 0.3 and 0.5, respectively (Narayan et al. 1996, 1997). $\beta_{\text{adv}} = 0.5$ corresponds to equipartition between magnetic and gas pressure, as suggested by the work of Balbus and Hawley (1991).

Unlike standard thin accretion disks, an ADAF is well approximated by a series of concentric spherical shells with the properties of the gas varying as a function of radius (Narayan & Yi 1995a). The self similar solution of Narayan and Yi (1994, 1995a) provides reasonably accurate analytical estimates of the properties of the accretion flow. For the present discussion, the quantities of interest are

$$\begin{aligned} \frac{v(r)}{c} &\simeq 0.37 \alpha r^{-1/2}, \\ \theta_p(r) &\simeq 0.09 \left(\frac{\beta_{\text{adv}}}{0.5} \right) r^{-1}, \\ n_e(r) &\simeq 6.3 \times 10^{19} \alpha^{-1} m^{-1} \dot{m} r^{-3/2} \text{ cm}^{-3}, \\ B &= 7.7 \times 10^8 \alpha^{-1/2} \left(\frac{1 - \beta_{\text{adv}}}{0.5} \right)^{1/2} m^{-1/2} \dot{m}^{1/2} r^{-5/4} \text{ Gauss}, \end{aligned} \quad (1)$$

where $v(r)/c$ is the radial velocity in units of the velocity of light, $\theta_p(r) = kT_p/m_p c^2$ is the dimensionless proton temperature, $n_e(r)$ is the number density of electrons, $B(r)$ is the magnetic field strength and $r = R/R_S$ is the radius in Schwarzschild units ($R_S = 2.95 \times 10^5 m \text{ cm}$). In equation (1), the fraction, f , of the viscously dissipated energy that is carried inward by the accreting gas is taken to be ~ 1 (Narayan et al. 1996).

2.2. Timescales

For the electrons or protons in an ADAF to remain thermal as they accrete, they must have sufficient time to redistribute their kinetic energy by various processes. We therefore take thermalization by Coulomb collisions to be efficient when the timescale for collisions between the electrons, t_{ee} , or between the protons, t_{pp} , is shorter than the accretion time, t_a . Since the protons are non-relativistic ($\theta_p < 0.1$) their thermalization time is (Spitzer, 1962)

$$\begin{aligned} t_{pp} &= \frac{(2\pi)^{1/2}}{n_p \sigma_T c \ln \Lambda} \left(\frac{m_p}{m_e} \right)^2 \theta_p^{3/2}, \\ &\simeq 9.2 \times 10^{-3} \alpha \left(\frac{\beta_{adv}}{0.5} \right)^{3/2} m \dot{m}^{-1} \text{ s}, \end{aligned} \quad (2)$$

where $n_p = n_e$ is the proton number density, σ_T is the Thomson cross-section, $\ln \Lambda \approx 20$ is the Coulomb logarithm, and we have used equation (1) for the proton temperature profile. The time required for the protons and electrons to reach thermal equilibrium is (Spitzer 1962)

$$\begin{aligned} t_{ep} &= \frac{(2\pi)^{1/2}}{2 n_e \sigma_T c \ln \Lambda} \left(\frac{m_p}{m_e} \right) (\theta_e + \theta_p)^{3/2}, \\ &\simeq 9.3 \times 10^{-5} \alpha \theta_e^{3/2} m \dot{m}^{-1} r^{3/2} \text{ s}. \end{aligned} \quad (3)$$

So long as the electrons are non-relativistic their timescale for thermalization is (Spitzer 1962)

$$\begin{aligned} t_{ee} &= \frac{(2\pi)^{1/2}}{n_e \sigma_T c \ln \Lambda} \theta_e^{3/2}, \\ &\simeq 1.0 \times 10^{-7} \alpha m \dot{m}^{-1} r^{3/2} \theta_e^{3/2} \text{ s}. \end{aligned} \quad (4)$$

For thermalization to occur before the gas falls into the central black hole, the above timescales must be less than the accretion time of the gas, which is

$$t_a = \int \frac{dR}{v(R)} \simeq 1.8 \times 10^{-5} \alpha^{-1} m r^{3/2} \text{ s}. \quad (5)$$

From these timescales we can readily estimate the critical accretion rate, \dot{m}_{crit} , above which the ADAF solution ceases to exist. For sufficiently large mass accretion rates, the electrons and protons become thermally well coupled and so the assumption of a two temperature plasma is no longer valid; the two temperature ADAF therefore no longer exists. The accretion rate above which this occurs is obtained by setting $t_{ep} \sim t_a$, which gives

$$\dot{m}_{crit} \approx 0.45 \alpha^2, \quad (6)$$

where we have set $\theta_e \sim 0.2$, which is valid for high \dot{m} systems (Mahadevan 1997). This is comparable to the critical accretion rates obtained by independent arguments (Narayan & Yi 1995b; see also Mahadevan 1997).

2.3. Proton Thermalization

To determine the accretion rates at which the protons have sufficient time to thermalize by Coulomb collisions, we set $t_{\text{pp}} \lesssim t_{\text{a}}$. This gives the requirement

$$\dot{m} \gtrsim 500 \alpha^2 \left(\frac{\beta_{\text{adv}}}{0.5} \right)^{3/2} r^{-3/2}. \quad (7)$$

Since the maximal accretion rate for an ADAF is \dot{m}_{crit} , the radius above which the protons can thermalize is

$$r_{\text{th}} \approx 100 \left(\frac{\beta_{\text{adv}}}{0.5} \right) \left(\frac{\dot{m}}{\dot{m}_{\text{crit}}} \right)^{-2/3}. \quad (8)$$

For a given \dot{m} , the protons are unable to redistribute their energy through Coulomb collisions for $r < r_{\text{th}}$ and so the proton distribution function at these radii is primarily determined by the viscous heating mechanism. Observational probes of the proton distribution function would therefore provide valuable information about the details of the viscous heating mechanism. Mahadevan et al. (1997) have shown that the γ -ray spectrum from pions created by proton collisions in ADAFs can be used as a direct probe of the proton distribution function, and can therefore provide a means of studying viscosity in hot accretion flows.

3. The Electron Distribution Function in ADAFs

In this section we analyze the form of the electron distribution function in ADAFs. We show that for moderately high accretion rates, Coulomb collisions and synchrotron self-absorption can efficiently thermalize the electrons, even in the high energy tail of the distribution function. At lower accretion rates, however, these processes are too inefficient, and the form of the distribution function depends on the dominant heating and cooling mechanisms of the electrons. This is discussed in §4.

3.1. Coulomb Collisions

The accretion rate, \dot{m}_{th} , above which the electrons can thermalize via Coulomb collisions is obtained by setting the timescale for electron–electron collisions, t_{ee} , equal to the accretion time, t_{a} , which gives

$$\dot{m}_{\text{th}} \approx 3.8 \times 10^{-4} T_9^{3/2} \alpha^2, \quad (9)$$

where T_9 is the electron temperature in units of 10^9 K. For $\dot{m} \gtrsim \dot{m}_{\text{th}}$, electrons with energies $\sim kT_e$ are thermal. Since most of the synchrotron emission from ADAFs comes from the high energy tail of the distribution (§4), it is also necessary to determine whether electrons with energies $\gg kT_e$ have enough time to thermalize. To investigate this, we use the Fokker–Planck equation which, for an isotropic energy distribution function, takes the form

$$\frac{\partial n(\gamma, t)}{\partial t} = -\frac{\partial}{\partial \gamma} \left[\left(\frac{d\gamma}{dt} \right) n(\gamma, t) \right] + \frac{1}{2} \frac{\partial^2}{\partial \gamma^2} \left[\frac{d(\Delta\gamma)^2}{dt} n(\gamma, t) \right], \quad (10)$$

where $n(\gamma, t)$ is the distribution function, $d\gamma/dt$ represents systematic acceleration, and $d(\Delta\gamma)^2/dt$ represents stochastic acceleration. The systematic acceleration is negative for particles with $\gamma \gtrsim \theta_e$, and positive for $\gamma \lesssim \theta_e$, which corresponds to slowing down (speeding up) particles with energies large (small) compared to the mean energy of the plasma. The stochastic acceleration is always positive and corresponds to diffusion in energy space.

The timescale for an electron with a Lorentz factor γ to thermalize with a background plasma of temperature θ_e is given roughly by the timescale on which the electron’s energy e-folds. This ensures that the electron interacts significantly with the plasma. The resulting timescale depends on γ and θ_e , and is obtained by determining whether systematic or stochastic acceleration dominates the energy changes of the electron.

The systematic acceleration of an electron with Lorentz factor γ , interacting with a thermal plasma of temperature θ_e , is given approximately by (Dermer & Liang 1989)

$$\frac{d\gamma}{dt} = -\frac{3}{2} n_e \sigma_{TC} \ln \Lambda \left[\frac{1}{A(\theta_e)} - \frac{1}{\gamma} \right], \quad (11)$$

where $A(\theta_e) = K_2(1/\theta_e)/K_1(1/\theta_e)$ and K_n is the modified Bessel function of order n . The timescale on which the electron’s energy e-folds is therefore

$$t_{\text{sys}}^e = \frac{1}{|d \ln \gamma / dt|} = \frac{2}{3} \frac{\gamma}{n_e \sigma_{TC} \ln \Lambda} \left| \frac{1}{A(\theta_e)} - \frac{1}{\gamma} \right|^{-1}. \quad (12)$$

Equations (11) and (12) are good analytical approximations to detailed numerical calculations provided that $\theta_e \gtrsim 0.3$ and $\gamma \gtrsim 2$ (Dermer & Liang 1989).

The stochastic acceleration is determined by substituting equation (11) into the Fokker-Planck equation, setting $\partial n / \partial t = 0$ (as is required for a thermal plasma) and solving the second order differential equation. The two integration constants in the resulting solution are determined by (1) requiring no net flux of electrons in energy space (since there are no sinks or sources of electrons) and (2) imposing the physical requirement that the stochastic acceleration not increase exponentially for large γ . This gives

$$\frac{d(\Delta\gamma)^2}{dt} = 3 n_e \sigma_{TC} \ln \Lambda \left[\frac{\theta_e}{A(\theta_e)} + \frac{\theta_e}{\gamma} z_{\theta_e} + \frac{\theta_e^2}{\gamma^2} z_{\theta_e} \right], \quad (13)$$

where $z_{\theta_e} = 2[\theta_e/A(\theta_e)] - 1$. The resulting diffusion time is

$$t_{\text{diff}}^e = 1 \left/ \frac{1}{\gamma^2} \frac{d(\Delta\gamma)^2}{dt} \right. = \frac{\gamma^2}{3 n_e \sigma_{TC} \ln \Lambda} \left[\frac{\theta_e}{A(\theta_e)} + \frac{\theta_e}{\gamma} z_{\theta_e} + \frac{\theta_e^2}{\gamma^2} z_{\theta_e} \right]^{-1}. \quad (14)$$

Since equations (13) and (14) are derived from equation (11), they are also only valid for $\theta_e \gtrsim 0.3$ and $\gamma \gtrsim 2$. We note that the stochastic acceleration derived here does not rise exponentially as indicated in Dermer & Liang (1989; cf. their eq. [14] and figure 2). More recent detailed calculations by Nayakshin & Melia (1997) agree with the analytic approximation for the stochastic acceleration given here.

Setting $(t_{\text{sys}}, t_{\text{diff}}) < t_a$ and using equations (1) and (5) gives the accretion rates required for thermalization,

$$\begin{aligned} \left(\frac{\dot{m}}{\alpha^2} \right)_{\text{sys}}^e &\gtrsim 1.4 \times 10^{-3} \gamma \left| \frac{1}{A(\theta_e)} - \frac{1}{\gamma} \right|^{-1}, \\ \left(\frac{\dot{m}}{\alpha^2} \right)_{\text{diff}}^e &\gtrsim 7.3 \times 10^{-4} \gamma^2 \left[\frac{\theta_e}{A(\theta_e)} + \frac{\theta_e}{\gamma} z_{\theta_e} + \frac{\theta_e^2}{\gamma^2} z_{\theta_e} \right]^{-1}. \end{aligned} \quad (15)$$

For electrons with energies comparable to the mean energy of the plasma, $\gamma \sim \theta_e$ and equation (12) shows that $t_{\text{sys}}^e \rightarrow \infty$; the electron, on average, is not heated by direct acceleration, but instead diffuses in energy space (as determined by the stochastic term). For large γ , $t_{\text{sys}}^e < t_{\text{diff}}^e$, and so electrons with energies much larger than the mean energy of the plasma, $\gamma \gg \theta_e$, first lose energy by direct cooling and then relax by diffusion. In order to assess the efficiency of thermalization, we therefore take the minimum of the systematic and diffusion timescales as the relevant timescale against which to compare the accretion time.

For a plasma at temperature θ_e , an electron with Lorentz factor γ can thermalize via Coulomb collisions if the accretion rate is greater than the smaller of the two accretion rates given in equation (15). The dashed lines in figure 1 show this accretion rate as a function of the Lorentz factor γ , for two values of θ_e . For accretion rates below these curves, the electrons do not have time to interact with one another via collisions and are “frozen” into their initial distribution. Unless other thermalization processes are important, this implies that the form of the distribution function can deviate substantially from a Maxwellian. We show below that because the synchrotron photons in ADAFs are highly self-absorbed, the electrons are able to thermalize at lower accretion rates (and higher γ) by interacting via the exchange of self-absorbed synchrotron photons.

3.2. Electron Thermalization Through Synchrotron Self-Absorption

Synchrotron self-absorption has been treated in the context of finding steady state power-law electron distributions (McCray 1969), heating low energy electrons through

self-absorption (Ghisellini et al. 1988), and as a thermalizing mechanism for low energy electrons (Ghisellini & Svensson 1990). In particular, Ghisellini and Svensson (1990) have shown that self-absorption of synchrotron photons leads to a thermal distribution of electrons over a large range of γ in a few synchrotron cooling times. The basic thermalization mechanism is energy exchange via the absorption and emission of synchrotron photons, which can be important even when the plasma is effectively collisionless.

In keeping with the analysis of the previous section we discuss thermalization induced by synchrotron self-absorption using the Fokker–Planck equation. Instead of attempting to solve the complete integrodifferential equation (eq. [10]), we check for consistency by assuming that the (thermal) synchrotron radiation is highly self-absorbed, and then determining whether the thermalization timescales obtained from the Fokker–Planck coefficients are faster than the accretion time.

The kinetic equation governing the electron distribution function can be written as a Fokker–Planck equation with coefficients given by (McCray 1969; Ghisellini et al. 1988)

$$\frac{d\gamma}{dt} = -\frac{1}{m_e c^2} \int_0^\infty j(\nu, \gamma) d\nu + \frac{1}{\gamma p} \frac{\partial}{\partial \gamma} [\gamma p C(\gamma)], \quad (16)$$

$$\frac{d(\Delta\gamma)^2}{dt} = 2 C(\gamma), \quad (17)$$

where

$$C(\gamma) \equiv \frac{1}{2m_e^2 c^2} \int_0^\infty \frac{I(\nu)}{\nu^2} j(\nu, \gamma) d\nu. \quad (18)$$

$j(\nu, \gamma)$ is the cyclo-synchrotron emissivity (ergs s⁻¹ Hz⁻¹), $p = \gamma\beta = (\gamma^2 - 1)^{1/2}$ is the electron's momentum in units of $m_e c$, and $I(\nu)$ is the intensity of the background photons (ergs cm⁻² s⁻¹ Hz⁻¹).

To evaluate $C(\gamma)$, we use three properties of synchrotron radiation in ADAFs. First, the electrons which are responsible for most of the synchrotron emission are from the high energy tail of the distribution. By multiplying the relativistic Maxwell–Boltzmann distribution by the synchrotron emissivity and using the method of steepest descent, we can determine the Lorentz factor (γ_{\max}) of the electron responsible for most of the emission. This gives

$$\gamma_{\max} = 2^{1/3} \theta_e x_M^{1/3} \sim 10 \theta_e, \quad (19)$$

where $x_M \sim 500$ and is a very weak function of \dot{m} (Mahadevan 1997). Large values of x_M , as is the case in ADAFs, imply that most of the observed synchrotron radiation originates in the exponential tail of the single particle emissivity. Since the electrons responsible for most of the synchrotron emission are relativistic (eq. [19]), we can evaluate $C(\gamma)$ by using the synchrotron formula for $j(\nu, \gamma)$ (Rybicki & Lightman 1979)

$$j(\nu, \gamma) = S_0 \sin \alpha_p F\left(\frac{\nu}{\nu_c}\right),$$

$$S_0 = \frac{3^{1/2}(2\pi)e^2\nu_B}{c}, \quad \nu_c = \frac{3}{2}\gamma^2\nu_B \sin \alpha_p, \quad \nu_B = \frac{eB}{2\pi m_e c}, \quad (20)$$

where α_p is the angle the electron makes with the magnetic field, $F(x)$ is an integral over modified Bessel functions (Rybicki & Lightman 1979, eq. [6.31c]), and $\nu_B = 2.8 \times 10^6 B$ Hz is the cyclotron frequency.

Second, an electron with Lorentz factor γ_{\max} emits most of its radiation at its critical frequency $\nu_c \simeq 1.5\gamma_{\max}^2\nu_B$. This radiation is, however, highly self-absorbed and becomes optically thin only at a frequency $\nu_t = 1.5\theta_e^2 x_M \nu_B \approx 4.7\nu_c$ (Narayan & Yi 1995b; Mahadevan 1997). We can therefore set $\nu_t \gg \nu_c$ to good approximation.

Finally, since the plasma is highly self-absorbed, the radiation field, $I(\nu)$, is Raleigh–Jeans at a temperature θ_e up to the frequency ν_t , where the plasma becomes optically thin (see Narayan & Yi 1995b; Mahadevan 1997). This gives

$$I(\nu) = \begin{cases} 2\nu^2 m_e \theta_e & 0 < \nu < \nu_t, \\ 0 & \nu > \nu_t. \end{cases} \quad (21)$$

Combining these properties, equation (18) becomes

$$\begin{aligned} C(\gamma) &= \frac{3^{1/2}e^3 B}{m_e^2 c^4} \theta_e \nu_c \int_0^{\nu_t/\nu_c} F(x) dx, \\ &\simeq 1.2 \times 10^{-9} B^2 \theta_e \gamma^2, \\ &\equiv C_1 B^2 \theta_e \gamma^2, \end{aligned} \quad (22)$$

where C_1 is a constant as defined above and we have averaged over all pitch angles.

Equations (16) and (17) are now easily evaluated to give the systematic and diffusion timescales,

$$\begin{aligned} t_{\text{sys}}^s &= \frac{1}{|d \ln \gamma / dt|} = \frac{1}{C_1 B^2 \gamma} \left| 1 - 4 \frac{\theta_e}{\gamma} \right|^{-1}, \\ t_{\text{diff}}^s &= 1 \left/ \frac{1}{\gamma^2} \frac{d(\Delta\gamma)^2}{dt} \right. = \frac{1}{2C_1 B^2 \theta_e}. \end{aligned} \quad (23)$$

Note that in the cyclotron limit, the systematic and stochastic coefficients can be evaluated by recognizing that $j(\nu, \gamma) \propto \delta(\nu - \nu_B)$, which yields

$$\begin{aligned} \frac{d\gamma}{dt} &\simeq 3C_1 B^2 \theta_e, \\ \frac{d(\Delta\gamma)^2}{dt} &\simeq C_1 B^2 \theta_e \gamma^2 \beta^2. \end{aligned} \quad (24)$$

In the limit $\beta \rightarrow 0$, the stochastic term is zero, and the electrons only heat up by absorbing radiation from the background field (Ghisellini & Svensson 1990). Since we are concerned with thermalization of high energy electrons, we neglect the cyclotron limit in our discussion.

Setting $(t_{\text{sys}}^s, t_{\text{diff}}^s) < t_a$, and using equations (1) and (5), gives the accretion rates at which thermalization by self-absorption of synchrotron photons is efficient

$$\begin{aligned} \left(\frac{\dot{m}}{\alpha^2}\right)_{\text{sys}}^s &\gtrsim 7.6 \times 10^{-5} \frac{1}{\gamma} \left|1 - 4\frac{\theta_e}{\gamma}\right|^{-1} \left(\frac{1 - \beta_{\text{adv}}}{0.5}\right)^{-1} r, \\ \left(\frac{\dot{m}}{\alpha^2}\right)_{\text{diff}}^s &\gtrsim 3.8 \times 10^{-5} \frac{1}{\theta_e} \left(\frac{1 - \beta_{\text{adv}}}{0.5}\right)^{-1} r. \end{aligned} \quad (25)$$

For a plasma of temperature θ_e , an electron with Lorentz factor γ can thermalize through synchrotron self-absorption if the accretion rate is greater than the smaller of the two accretion rates given in equation (25). The solid lines in figure 1 show this accretion rate as a function of the Lorentz factor γ for two values of θ_e at $r = 10$. For fixed θ_e , these curves can be scaled linearly with r for other radii (cf. eq. [25]). As Figure 1 indicates, synchrotron self-absorption is significantly more efficient than Coulomb collisions at thermalizing high energy electrons.

Note that unlike electron thermalization, thermalization by synchrotron self-absorption depends explicitly on the radius. The magnetic field is weaker at larger radii which, for a fixed temperature, decreases the amount of synchrotron radiation. This decreases the amount of self-absorption in the plasma and so thermalization is less efficient, as is clear from equation (25).

The systematic term in equation (25) is the dominant thermalizing mechanism for electrons with $\gamma \sim \gamma_{\text{max}}$. This term can be rewritten to give a condition on the radius below which the plasma is thermal,

$$r_{\text{th}}^e \sim 1.3 \times 10^4 \gamma \left(\frac{\dot{m}}{\alpha^2}\right), \quad (26)$$

where we have taken $\gamma \gg \theta_e$. For a given γ and \dot{m}/α^2 , the electrons are thermal for all radii $r \lesssim r_{\text{th}}^e$. To determine the accretion rates above which electrons with $\gamma \sim \gamma_{\text{max}}$ are thermal throughout the flow, we set $\gamma \simeq 10\theta_e$ and $r_{\text{th}}^e \simeq 1000$ in equation (26), which gives

$$\frac{\dot{m}}{\alpha^2} \gtrsim 8 \times 10^{-3} \theta_e^{-1} \simeq 4 \times 10^{-2}, \quad (27)$$

In the last equality, we have set $\theta_e \sim 0.2$, as is valid for high accretion rates (Mahadevan 1997). To determine the accretion rates at which the electrons cannot thermalize anywhere in the ADAF, we set $r_{\text{th}}^e \sim 10$ and obtain

$$\frac{\dot{m}}{\alpha^2} \lesssim 10^{-4} \theta_e^{-1} \simeq 10^{-4}, \quad (28)$$

where we have set $\theta_e \sim 1$, which is valid at small radii for low accretion rates (§4.2). For these low accretion rates, the electrons responsible for most of the synchrotron emission are unable to thermalize throughout the accretion flow, and the assumption of thermal synchrotron radiation is no longer valid. The form of the electron distribution function

and the resulting synchrotron spectrum at these low accretion rates are determined in §4 and §5.

For accretion rates between these extremes, $10^{-4} \lesssim \dot{m}/\alpha^2 \lesssim 4 \times 10^{-2}$, the electrons will be thermal at small radii where synchrotron self-absorption is efficient, but will not necessarily be thermal at larger radii. The implications of this are considered in §6.

To conclude this section, we note that the above analysis breaks down for electrons with large Lorentz factors ($\gamma \gg \gamma_{\text{max}}$). This is because the radiation produced from these electrons is not self-absorbed, and escapes the plasma freely. The critical Lorentz factor, γ_{crit} , at which this occurs is estimated by setting the electron's critical frequency equal to the frequency at which the plasma becomes optically thin, $\nu_t = 1.5\gamma_{\text{crit}}^2\nu_B$. This gives

$$\gamma_{\text{crit}} = \theta_e x_M^{1/2}, \quad (29)$$

which is always greater than γ_{max} for ADAFs since $\gamma_{\text{crit}} = 2^{-1/3}x_M^{1/6}\gamma_{\text{max}} \gtrsim 2\gamma_{\text{max}}$.¹ For electrons with $\gamma > \gamma_{\text{crit}}$ the stochastic Fokker-Planck coefficient (cf. eq.[17]) is zero, since there is no absorption, and the systematic term is due solely to optically thin synchrotron cooling (cf. eq.[16] with $C(\gamma) = 0$). The electron distribution for $\gamma > \gamma_{\text{crit}}$ is therefore not necessarily thermal. This, however, has little effect on the synchrotron spectrum since most of the emission comes from electrons with $\gamma \approx \gamma_{\text{max}} < \gamma_{\text{crit}}$.

4. Heating and Cooling of Electrons

When thermalization by Coulomb collisions and synchrotron self-absorption is inefficient, the evolution of the electron distribution function is determined by the interplay between the dominant heating and cooling mechanisms. These can be determined by considering the electron energy equation

$$\begin{aligned} \rho T v \frac{ds}{dR} &= n v \frac{d\epsilon}{dR} - q^c = q^{e+} - q^-, \\ q^c &\equiv k T v \frac{dn}{dR}, \\ q^{e+} &= q^{\text{ie}} + q^v, \end{aligned} \quad (30)$$

where s is the entropy of the electrons per unit mass of the gas, ϵ is the internal energy of the electrons per unit mass, q^c is the compressive heating (or cooling) rate per unit volume, and q^- is the energy loss due to radiative cooling. The total external heating

¹However for accretion rates below $\sim 10^{-9}$ the plasma is no longer self-absorbed and there is no thermalization by synchrotron self-absorption ($\gamma_{\text{crit}} < \gamma_{\text{max}}$ since $x_M < 1$).

of the gas, q^{e+} , is a sum of the heating via Coulomb collisions with the hotter protons, q^{ie} , and direct viscous heating, q^v .

Much of the previous work on ADAFs has neglected the compressive heating of electrons and has assumed that the electron temperature profile is given by solving $q^- = q^{e+}$ (e.g., Narayan & Yi, 1995b). We show below that this is likely to be a poor approximation except for systems near the critical accretion rate. This point has already been made by Nakamura et al. (1997), who first recognized the importance of compressive heating in determining the electron temperature profile.

As long as $q^{e+} \ll q^c$ and $q^- \ll q^c$, the right hand side of equation (30) is small compared to each term on the left hand side. All of the compressive heating therefore goes into changing the internal energy of the gas, with nearly constant entropy. We now show that both of these conditions are satisfied at low accretion rates, so that the electrons in ADAFs compress adiabatically as they accrete onto the central object.

4.1. Heating

The dominant heating mechanism for the electrons is obtained by comparing the relative magnitudes of q^c , q^{ie} , and q^v . Using equations (1) and (30), the compressive heating rate is

$$q^c \simeq 5 \times 10^{17} \dot{m} m^{-2} T_9 r^{-3} \text{ erg cm}^{-3} \text{ s}^{-1}. \quad (31)$$

The energy transfer rate between protons and electrons via Coulomb collisions is (Stepney & Gilbert 1983)

$$\begin{aligned} q^{ie} &\simeq 2.05 \times 10^{-17} n_e n_i (T_i - T_e) T_e^{-3/2} \\ &= 2.5 \times 10^{21} \alpha^{-2} \dot{m}^2 m^{-2} T_9^{-3/2} r^{-4} \text{ erg cm}^{-3} \text{ s}^{-1}, \end{aligned} \quad (32)$$

where we have assumed that $T_e \leq 10^{10} \text{K}$ so that a non-relativistic formula is reasonably accurate. The last equality follows from using equation (1), and setting $T_e \ll T_i$, $n_e = n_i$.

The viscous heating of the electrons is determined by allowing for a fraction $\delta \sim m_e/m_p \approx 1/2000$ of the viscously generated energy to be transferred directly to the electrons, so that (Mahadevan 1997)

$$q^v \simeq 3 \times 10^{17} \dot{m} m^{-2} r^{-4} \delta_o \text{ erg cm}^{-3} \text{ s}^{-1}, \quad (33)$$

where $\delta_o = 2000\delta$. Both compressive and viscous heating are proportional to the accretion rate and their ratio is given by

$$q^c/q^v \sim 2 \delta_o^{-1} T_9 r, \quad (34)$$

which is independent of the global parameters of the ADAF. In the inner regions of the accretion flow ($r \sim 3$), $T_9 \sim 5$, while for larger radii the temperature decreases roughly as $r^{-2/3}$ (§4.2). Compressive heating of the electrons is therefore always more important than direct viscous heating provided that δ is not substantially larger than 10^{-3} .

Coulomb heating of the electrons by the protons is, however, a two body process and becomes less important for small \dot{m} . From the expressions for q^c and q^{ie} given above, it follows that compressive heating dominates over Coulomb heating provided that

$$\dot{m} \lesssim 2 \times 10^{-4} \alpha^2 T_9^{5/2} r. \quad (35)$$

Comparing this with equations (15) and (25) shows that for low \dot{m} , where both Coulomb collisions and synchrotron self-absorption are unable to thermalize the plasma, compressive heating is the dominant heating mechanism.

4.2. Cooling

Synchrotron cooling can be an important energy loss mechanism in ADAFs because of the assumption of near equipartition magnetic fields. In fact, for the low mass accretion rates of interest here, synchrotron radiation is the dominant source of cooling (Narayan & Yi, 1995b; Mahadevan 1997). In §2 we showed that the thermalization time through synchrotron self-absorption is of order the electron cooling time and that self-absorption is inefficient at thermalizing the electrons for $\dot{m} \lesssim 10^{-4} \alpha^2$ (cf. Figure 1). For these low accretion rates electrons therefore cannot radiate a significant fraction of their energy in an accretion time. Since the dominant source of the electron’s energy is compressive heating (q^c) this implies that $q^- \ll q^c$.

This argument relies on the accuracy of our estimate of the electron temperature in the accretion flow, since higher temperatures would lead to more efficient synchrotron cooling. Since previous work has neglected compressive heating, however, we must verify that electron temperatures of $\sim 10^9$ K are still valid when the electron temperature profile is determined by adiabatic compression.

For adiabatic compression, the temperature profile is given by $T \propto \rho^{\Gamma-1}$, where Γ is the ratio of the gas specific heats and $\rho \propto r^{-3/2}$. Since the internal energy of the electron gas includes a contribution from the magnetic field energy, $\Gamma = (8 - 3\beta_{\text{adv}})/(6 - 3\beta_{\text{adv}})$ for non-relativistic electrons (Esin 1997). For an equipartition magnetic field, $\Gamma = 13/9$, which gives a temperature profile of $T \propto r^{-2/3}$. $\Gamma = 4/3$ is still valid in the relativistic limit, in which case $T \propto r^{-0.5}$. For $T_e \approx T_p$ at $r \approx 10^4$, the above scalings imply that the electron temperature near the last stable orbit is $\approx 5 \times 10^9$ K, which is comparable with previous estimates.

4.3. The Distribution Function of an Adiabatically Compressed Gas

For $\dot{m} \lesssim 10^{-4}\alpha^2$, Coulomb collisions and synchrotron self-absorption are unable to thermalize the electrons. The electrons therefore do not interact with one another and can be well approximated as a collisionless gas. Furthermore, at these low accretion rates, the electrons compress nearly adiabatically as they accrete onto the central object.

An adiabatic change is one in which the properties of a system vary slowly compared to the characteristic timescales of the system. During such a change, the system’s phase space volume is a conserved quantity (Landau & Lifshitz, *Mechanics* §49). We use this property to determine the evolution of the distribution function of a collisionless electron gas subjected to adiabatic changes in its volume. We emphasize that the discussion which follows is not specific to an ADAF, but applies to any collisionless plasma which undergoes adiabatic changes.

The adiabatic compression of a collisionless gas can be viewed as the independent adiabatic compression of each particle in the gas, since there is no coupling between the particles. By adiabatic invariance, the quantity $p^3\rho^{-1}$ is conserved for each particle in a monatomic gas, where p is the momentum of the particle and ρ is the density of the gas.² The evolution of the distribution function is therefore given by the transformation $p \rightarrow ap$, where $a = (\rho_f/\rho_i)^{1/3}$, and $\rho_{i(f)}$ denotes the initial (final) gas density. We emphasize that this transformation is valid for all momenta p , both non-relativistic and relativistic.

To determine how the distribution function of a non-relativistic thermal gas of temperature θ_e changes under an adiabatic compression, consider the Maxwell–Boltzmann distribution function

$$n(p)dp = \frac{4\pi p^2}{(2\pi m^2 c^2 \theta_e)^{3/2}} \exp\left(-\frac{p^2}{2m^2 c^2 \theta_e}\right) dp. \quad (36)$$

For now, assume that the compression factor, a , is such that the particle momenta after compression remain non-relativistic. Substitution of the transformation $p \rightarrow ap$ into equation (36) shows that the form of the distribution function remains the same. The gas is still thermal, but is now characterized by a temperature $\theta'_e = a^2\theta_e = (\rho_f/\rho_i)^{2/3}\theta_e$, which is the usual result for the adiabatic compression of a $\Gamma = 5/3$ gas. A thermal distribution is therefore maintained even though the gas is collisionless.

Similarly, for a relativistic thermal gas characterized by the Maxwell–Boltzmann distribution function,

$$n(p)dp = \frac{p^2}{m^3 c^3 \theta_e K_2(1/\theta_e)} \exp\left(-\frac{p}{m c \theta_e}\right) dp \quad (37)$$

² $p^3\rho^{-1}$ is also the adiabatic invariant for particles moving in an isotropically tangled, flux frozen, magnetic field.

setting $p \rightarrow ap$ and assuming that the final momenta are relativistic shows that the gas remains thermal with a final temperature $\theta'_e = a\theta_e = (\rho_f/\rho_i)^{1/3}\theta_e$. This is the usual result for the adiabatic compression of a $\Gamma = 4/3$ gas.

Under adiabatic compression, an initially non-relativistic (relativistic) thermal gas therefore remains a non-relativistic (relativistic) thermal gas, as long as the post compression momenta remain non-relativistic (relativistic). Consider, however, a non-relativistic thermal gas (eq. [36]), which is compressed by a sufficient amount that the final momenta of the particles are now relativistic. Since the transformation $p \rightarrow ap$ is valid regardless of the magnitude of the momenta, the post compression distribution function is given by

$$n(p)dp = \frac{4\pi p^2}{(2\pi m^2 c^2 a^2 \theta_e)^{3/2}} \exp\left(-\frac{p^2}{2m^2 c^2 a^2 \theta_e}\right) dp. \quad (38)$$

This has the form of a non-relativistic Maxwellian, even though the particle energies can be highly relativistic. Therefore a collisionless gas which is adiabatically compressed across the non-relativistic/relativistic boundary does not maintain a thermal distribution.³ In particular, the relativistic high energy tail of the adiabatically compressed distribution function falls off as a Gaussian rather than as an exponential (cf. eqs. [38], [37]).

In order to assess the implications of this new distribution function, we compare it with a thermal distribution function which has the same average energy (the “best fit” thermal distribution). The average energy of an adiabatically compressed gas in the relativistic limit is (in units of $m_e c^2$)

$$\begin{aligned} \langle \gamma \rangle &= \frac{4\pi}{(2\pi a^2 \theta_e)^{3/2}} \int_0^\infty \gamma^3 \exp\left(-\frac{\gamma^2}{2a^2 \theta_e}\right) d\gamma, \\ &= \frac{4}{(2\pi)^{1/2}} a \theta_e^{1/2}. \end{aligned} \quad (39)$$

The average energy of the gas increases as a in the relativistic regime, rather than as a^2 as in the non-relativistic regime. Since the average energy of a thermal relativistic gas is $\langle \gamma \rangle = 3\theta_{MB}$, the “best fit” thermal gas has

$$\theta_{MB} = \left(\frac{8}{9\pi}\right)^{1/2} a \theta_e^{1/2}. \quad (40)$$

Figure 2a shows the distribution function for a gas which is adiabatically compressed by a factor of $a = 20$, from an initially thermal distribution with $\theta_e = 0.01$. Superimposed in the figure is the distribution function for a thermal gas which has the

³Note that for photons, which are massless, there is no such boundary, and so adiabatic changes always maintain a thermal distribution, a result which is, of course, well known in cosmology.

same mean energy as the adiabatically compressed gas ($\theta_{MB} \simeq 1$). As expected, the high energy tail of the adiabatically compressed gas is strongly suppressed with respect to the thermal gas.

A relativistic collisionless gas that adiabatically expands across the relativistic/non-relativistic boundary will also not maintain a thermal distribution. Fig 2b shows the distribution function for a gas which adiabatically expands by a factor of $a = 0.01$ from an initially thermal distribution with $\theta_e = 10$. Superimposed in the figure is the distribution function for a thermal gas which has the same mean energy ($\theta_{MB} \simeq 0.04$). The high energy tail of the adiabatically expanded gas is overpopulated with respect to the thermal gas since the distribution function falls off as an exponential, rather than as a Gaussian, in the non-relativistic limit.

Finally, we note that it is not necessarily valid to assume that the electrons have an adiabatically compressed distribution function just because thermalization is inefficient. This is because the timescale for thermalization as determined in §3 is not the same as the timescale on which an initially non-thermal distribution function changes substantially. As we discuss in Appendix C, it is only strictly true that the electrons have the adiabatically compressed distribution function out to $\gamma \sim \gamma_{\max}$ if the accretion rate is ~ 10 times smaller than the thermalization accretion rate given in §3 (cf. eqs. [25]). However, to accurately determine the form of the distribution function in this regime requires solving the complete Fokker-Planck equation, which is beyond the scope of this paper. In what follows, we assume that, for this narrow range in accretion rates, the electrons are well approximated as having an adiabatically compressed distribution function.

5. The Synchrotron Spectrum from an Adiabatically Compressed Gas

For an adiabatically compressed gas the large decrease in the number of particles at high energies has important consequences for the synchrotron emission from ADAFs. This is because most of the synchrotron emission originates from high energy electrons in the tail of the Maxwell-Boltzmann distribution. A lack of these high energy electrons will substantially reduce the synchrotron luminosity.

To determine the synchrotron emission from this new distribution, we first calculate the synchrotron source function, S_ν , and then calculate the emergent intensity. In the present analysis, we assume that all of the electrons are relativistic so that the distribution function (eq. [38]) takes the form

$$n(\gamma) d\gamma = \frac{4\pi}{(2\pi a^2 \theta_e)^{3/2}} \gamma^2 \exp\left(-\frac{\gamma^2}{2 a^2 \theta_e}\right) d\gamma. \quad (41)$$

Using equation (20), the emissivity, $\epsilon(\nu)_{\text{AC}}$, and the absorption coefficient, $\alpha(\nu)_{\text{AC}}$, are given by

$$\begin{aligned}\epsilon(\nu)_{\text{AC}} d\nu &= \int j(\nu, \gamma) n(\gamma) d\gamma, \\ &= E_0 \frac{\chi}{a^2 \theta_e} I'(x'_M, 2) d\nu \quad \text{ergs s}^{-1} \text{ Hz}^{-1},\end{aligned}\quad (42)$$

$$\begin{aligned}\alpha(\nu)_{\text{AC}} d\nu &= -\frac{1}{8\pi m_e \nu^2} \int \gamma p j(\nu, \gamma) \frac{\partial}{\partial \gamma} \left[\frac{n(\gamma)}{\gamma p} \right] d\gamma, \\ &= E_1 \frac{\chi^{-1}}{(a^2 \theta_e)^{3/2}} I'(x'_M, 3) d\nu \quad \text{cm}^{-1},\end{aligned}\quad (43)$$

where $p \rightarrow m_e \gamma c$ in the last equality. We have defined

$$\begin{aligned}I'(x, n) &= \frac{1}{4\pi} \int I\left(\frac{x}{\sin \alpha_p}, n\right) d\Omega_p, \\ I(x, n) &\equiv \frac{1}{x} \int_0^\infty F\left[\frac{x}{z^2}\right] z^n \exp(-z^2) d\gamma,\end{aligned}$$

and

$$E_0 \equiv \frac{8\pi^{1/2} e^2 \nu_B}{\sqrt{3}c}, \quad E_1 \equiv \frac{2^{1/2} e^2}{\sqrt{3\pi} c m_e \nu_B}, \quad x'_M \equiv \frac{\chi}{3 a^2 \theta_e}, \quad \chi \equiv \frac{\nu}{\nu_B}, \quad (44)$$

to maintain a similarity between the equations presented here and those for thermal synchrotron emission (Pacholczyk 1970; see also Mahadevan et al. 1996). $I'(x'_M, n)$ is $I(x'_M, n)$ integrated over all particle directions. The asymptotic expansions for $I(x'_M, n)$ and $I'(x'_M, n)$ at large and small x'_M are given in Appendix A.

The source function is determined using the limiting expressions for $I'(x, n)$ (Appendix A), which gives

$$S_\nu = \frac{\epsilon(\nu)_{\text{AC}}}{4\pi \alpha(\nu)_{\text{AC}}} = \begin{cases} 2^{1/2} m_e \nu^2 (a^2 \theta_e)^{1/2} & x'_M \ll 1, \\ 2^{1/2} 3^{1/4} m_e \nu_B^{1/4} \nu^{7/4} (a^2 \theta_e)^{3/4} & x'_M \gg 1. \end{cases} \quad (45)$$

The source function for a thermal gas in the Raleigh–Jeans limit is $S_\nu = 2m_e \nu^2 \theta_e$. For low frequencies, $x'_M \ll 1$, the source function for the adiabatically compressed gas has the same frequency dependence as that of a thermal gas, but the normalization is larger by a factor of $3\sqrt{\pi}/4 \simeq 1.33$ because there is an excess of low energy electrons (see Figure 2a). For large frequencies, $x'_M \gg 1$, however, the frequency dependence of the source function for the adiabatically compressed gas is different than that of a thermal gas, and varies as $\nu^{7/4}$.

The emissivity for an adiabatically compressed gas at large frequencies is given by

$$\epsilon(\nu)_{\text{AC}} d\nu = 1.6 \times 10^{-28} \nu_B x'_M{}^{3/4} \exp(-2x'_M{}^{1/2}) d\nu, \quad \text{ergs s}^{-1} \text{ Hz}^{-1}, \quad (46)$$

where we have used the expression for $I'(x'_M, n)$ for $x'_M \gg 1$ (Appendix A). For a thermal gas, the corresponding emissivity is (Mahadevan et al. 1996, eqs. [11], [A10]),

$$\epsilon(\nu)_{\text{Th}} d\nu = 3.4 \times 10^{-28} \frac{\theta_e^2 \nu_B}{K_2(1/\theta_e)} x'_M{}^{5/6} \exp(-1.8899 x'_M{}^{1/3}) d\nu, \quad \text{ergs s}^{-1} \text{ Hz}^{-1}, \quad (47)$$

where

$$x_M \equiv \frac{2\chi}{3\theta_e^2}.$$

The primary difference in the emissivity is the frequency dependence in the exponential. The exponential in the thermal spectrum falls off as $\nu^{1/3}$, while it falls more rapidly, as $\nu^{1/2}$, for an adiabatically compressed gas. This is expected because there is a lack of high energy particles in the adiabatically compressed gas as compared to a thermal gas with the same average energy.

Figure 3a compares the total synchrotron luminosity from a sphere of radius R for a thermal and an adiabatically compressed electron gas with the same average energy ($\theta_e = 0.5$ for the thermal gas). We set $R \simeq 7 \times 10^{11}$ cm, $B \simeq 200$ Gauss, and $n_e \simeq 10^{10}$ cm $^{-3}$, which are the parameters at ten Schwarzschild radii for a 2×10^6 solar mass black hole accreting at $\dot{m} \simeq 10^{-5}$. The solid line shows the spectrum for the adiabatically compressed gas, the dashed line shows the spectrum for the thermal gas, and the dotted line shows the optically thin emission that would result in each case were the plasma not self-absorbed. The adiabatically compressed gas has a significantly smaller synchrotron luminosity and becomes optically thin at a much lower frequency than the thermal gas. The adiabatically compressed gas is, however, still highly self-absorbed, thus validating our assumption that most of the emission comes from the exponential tail of the single particle emissivity.

Since the electron number density and magnetic field strength vary with radius, the total synchrotron spectrum from an ADAF is obtained by summing the individual spectrum from each radius in the accretion flow (e.g., Narayan & Yi, 1995b). An example of this is shown in Figure 3b for an adiabatically compressed gas (solid line) and a thermal gas (dashed line), taking $m = 2 \times 10^6$, $\dot{m} = 10^{-5}$, and using equation (1) for the number density and magnetic field as a function of radius. In this calculation, we have assumed for simplicity, and for comparison with previous work, that the internal energy of the electrons is constant throughout the accretion flow ($\theta_e = 0.5$ for the thermal gas). As Fig. 3b shows, the total luminosity from the adiabatically compressed gas is much lower than that of the thermal gas since there are fewer high energy electrons. The slope of the spectrum is, however, the same for the thermal and adiabatically compressed gases because both are highly self-absorbed and have very similar source functions.

The assumption of constant electron internal energy is valid at high \dot{m} where the cooling is efficient, as has been demonstrated by a number of previous calculations (e.g. Narayan & Yi, 1995b). For the lower accretion rates of interest here, where adiabatic compression determines the electron temperature profile, a constant electron temperature is an invalid assumption. Future calculations of synchrotron emission from low \dot{m} systems must self consistently calculate the evolution of the electron internal energy during adiabatic compression. The details of this calculation are given in Appendix B.

Finally, we note that the slope of the synchrotron spectrum in high \dot{m} ADAFs is

very similar to the characteristic radio slope observed in many black hole candidates (Mahadevan 1997). This is, however, a direct consequence of the assumed constancy of θ_e , which is not in general valid. Therefore we expect that low \dot{m} ADAFs will have (1) an unexpectedly low radio luminosity because of the absence of high energy electrons in the distribution function and (2) a radio slope that differs from that of high \dot{m} systems because the assumption of constant electron internal energy is no longer valid.

6. Discussion & Conclusions

In an advection dominated accretion flow, the timescale for protons and electrons to exchange energy by Coulomb collisions is sufficiently long compared to the accretion time that the two species are essentially decoupled. The protons and electrons can therefore have different temperatures and, if non-thermal, different distribution functions. The precise form of the electron and proton distribution functions is crucial for comparing calculated spectra from ADAFs with observations.

Coulomb collisions among the protons are too inefficient to force the protons to be thermal, since the timescale for thermalization is much longer than the accretion time (§2). The proton distribution function is therefore determined by the viscous heating mechanism, which is unknown. Since the protons are marginally relativistic, Mahadevan et al. (1997) have shown that an ADAF produces a substantial γ -ray flux, which is created from the decay of neutral pions produced through proton-proton collisions. In particular, they have shown that the luminosity and shape of the gamma-ray spectrum differs dramatically if the protons have a thermal or a power-law distribution. Comparison of the predicted γ -ray spectrum with observations can therefore determine the form of the proton distribution function and, in principle, provide a means of understanding the viscous heating mechanism in hot accretion flows. Mahadevan et al. (1997) have shown that the EGRET observations of the source 2EG J1746–2852 (Merck et al. 1996), which is coincident with the Galactic Center Sgr A*, are in good agreement with the predicted γ -ray spectrum from an ADAF, provided that the protons have a power-law distribution of the form $E^{-2.75}$. This is similar to the cosmic-ray proton energy distribution, which leads to the speculation that the heating mechanism responsible for accelerating cosmic rays might also be at work in ADAFs.

We have considered thermalization of electrons through both Coulomb collisions and self-absorbed synchrotron radiation. The latter process is significantly more important, since it can operate even when the electrons are effectively collisionless. We find that, for high accretion rates, $\dot{m} \gtrsim 4 \times 10^{-2} \alpha^2$, the electrons can efficiently exchange energy throughout the ADAF by both Coulomb collisions and the absorption and emission of synchrotron photons (§3). To conclude from this that the electrons are thermal also requires that thermalization proceed on a shorter timescale than the heating/cooling

of the electrons. This ensures that the electron distribution function can relax to a Maxwellian more rapidly than the heating/cooling induces modifications in the distribution function. Since synchrotron radiation is the dominant cooling mechanism, and also leads to thermalization because it is highly self-absorbed, this criterion is trivially satisfied for the cooling of the electrons in ADAFs.

Modifications of the electron distribution function by heating are perhaps a more viable concern. For the high mass accretion rates where thermalization appears to be efficient ($\dot{m} \gtrsim 4 \times 10^{-2} \alpha^2$), the electrons are primarily heated by Coulomb collisions with the hotter protons, provided that most of the viscously generated energy is transferred to the protons (§4.2). Since electron heating by the protons occurs on a timescale long compared to the thermalization timescale by electron-electron Coulomb collisions (§2.2), which is in turn long compared to the thermalization timescale by synchrotron self-absorption (§3.2), we conclude that heating of the electrons by the protons will not significantly modify the electrons from a thermal distribution.⁴ Therefore, for $\dot{m} \gtrsim 4 \times 10^{-2} \alpha^2$, where self-absorbed synchrotron radiation allows for efficient energy exchange among the electrons throughout the accretion flow, the electrons are likely to be thermal.

We find that for lower accretion rates, $\dot{m} \lesssim 10^{-4} \alpha^2$, thermalization is inefficient throughout the ADAF and thus the electrons are not necessarily thermal. In this regime, the heating and cooling mechanisms determine the electron distribution function. At these low accretion rates, cooling is very inefficient and compressive heating of the electrons is the dominant heating mechanism (§4). The evolution of the electron distribution function is therefore determined by adiabatic compression. Using the principle of adiabatic invariance, we find that the electron distribution function evolves by the transformation $p \rightarrow ap$, where p is the electron momenta (relativistic *or* non-relativistic) and a is a function of the electron density. For ADAFs, in which the internal energy of the gas contains a contribution from the magnetic field energy, the expression for the compression factor, a , is more complicated than that given in §4.3. The precise form of $a(\rho)$ does not, however, effect any of the conclusions of this paper. Nonetheless, in Appendix B we derive the form of $a(\rho)$ under the assumption that the magnetic field always contributes a constant fraction of the total pressure.

The above transformation for the electron momenta under adiabatic compression yields the distribution function given in equation (38), which is non-thermal if the electrons have relativistic energies. In particular, the high energy tail of an adiabatically compressed (expanded) gas is strongly suppressed (enhanced) with respect to a thermal

⁴Nonthermal heating of the electrons by wave-particle interactions, reconnection, etc. could, perhaps, modify the electrons from a thermal distribution. We have, however, as mentioned in the introduction, restricted our analysis to those processes whose role in ADAFs is relatively well understood, and so have not considered these effects. In addition, we note that the applicability of some of these non-thermal heating mechanisms to the nearly collisionless plasma in ADAFs is unclear.

gas of the same average energy (cf. Fig. 2). We emphasize that this is not specific to an ADAF. Any collisionless plasma which undergoes an adiabatic change will have a non-thermal distribution function if the particles’ momenta cross the relativistic/ non-relativistic boundary.

Our derivation of the distribution function of an adiabatically compressed electron gas is based on the assumption that the electrons are thermal at large radii. In many models where ADAFs have been successfully applied, the ADAF forms from a thin accretion disk at $r \sim 10^4$ (Narayan, McClintock, & Yi 1996). In this case, the electron distribution function is Maxwellian at large radii by virtue of the low temperature and large density in the thin accretion disk (cf. eq. [9]). In the event that an accretion disk is not present, as may be the case for super massive black holes at the centers of elliptical galaxies which accrete the surrounding gas through Bondi accretion, the gas at large radii is probably still thermal. This follows from the X-ray gas profiles of the centers of elliptical galaxies, which indicates that the gas is thermal with a temperature $\sim 10^{7.5}$ K (eg. Trinchieri et al. 1988).

For accretion rates such that $10^{-4} \lesssim (\dot{m}/\alpha^2) \lesssim 4 \times 10^{-2}$ the electrons are thermal for only part of the accretion flow. The initially thermal electron gas is adiabatically compressed down to a radius $\sim r_{\text{th}}^e$ (cf. eq. [26]), with no means of thermalizing by synchrotron self-absorption or Coulomb collisions. For $r \lesssim r_{\text{th}}^e$, however, electron thermalization by synchrotron self-absorption becomes efficient because the magnetic field is stronger and there is more synchrotron radiation in the plasma.

As the accreting gas passes through the “transition” radius, r_{th}^e , the electrons switch from an adiabatically compressed distribution function to a thermal one. This may substantially modify the predicted spectra from some ADAFs. For emission mechanisms in which the bulk of the emission comes from electrons with roughly the mean energy of the plasma, such as bremsstrahlung, the modified distribution function is unlikely to have a pronounced effect on the spectrum. Synchrotron radiation, on the other hand, is highly self-absorbed, with most of the emission coming from electrons in the high energy tail of the distribution function. Therefore, even when the mean electron energy is non-relativistic, the non-thermal distribution function due to adiabatic compression modifies the synchrotron spectrum substantially. In §5 we explicitly calculated the synchrotron spectrum from an adiabatically compressed electron gas. The synchrotron luminosity can be significantly smaller than that of a thermal electron gas with the same energy because there is a deficit of high energy particles in the tail of the distribution function (cf. Fig. 3). We note that, while the applications in this paper have been to ADAFs, the synchrotron emissivity and source function calculated in §5 apply to any adiabatically compressed gas.

Previous work in calculating the spectra from ADAFs has assumed that the electrons are thermal at all radii. These systems include A0620, V404Cyg (Narayan et al. 1996), and NGC 4258 (Lasota et al. 1996), where the accretion rates all satisfy

$\dot{m} \gtrsim 10^{-2}\alpha^2$. At these high accretion rates the assumption of thermal electrons is reasonably valid and the predicted spectra from these systems is unchanged by the present work. For systems with lower accretion rates, however, the change in the distribution function described here might considerably modify the predicted spectrum.

In particular, the ADAF model of Sgr A* (Narayan et al. 1995) should be reexamined since the estimated accretion rate falls below $10^{-2}\alpha^2$. Narayan et al. (1995) obtained good agreement with the observed spectrum of Sgr A* using $m = 7 \times 10^5$, $\dot{m} \simeq 3 \times 10^{-3}\alpha^2$, and an equilibrium temperature of $\theta_e \sim 1.5$. Using these parameters and equation (26) gives $r_{\text{th}}^e \simeq 600$. For $r \lesssim 600$ the assumption of thermal electrons is no longer valid. Since each frequency in the radio spectrum corresponds to emission from a particular radius, $\nu \propto r^{-5/4}$ (Mahadevan 1997), and the maximum synchrotron frequency for Sgr A* is $\sim 10^{12}$ Hz (Narayan et al. 1995), the emission from $r \gtrsim 600$ corresponds to frequencies $\lesssim 10^9$ Hz. For these frequencies the model of Narayan et al. (1995) may be inconsistent, but since almost all of the data is for $\nu \gtrsim 10^9$ Hz (see Fig. 1 in Narayan et al. 1995), the possibility of non-thermal electrons is unlikely to be important for this system.

A more promising application of the present work is in modeling the $3 \times 10^7 M_\odot$ black hole in M31 (Kormendy & Richstone 1995). The accretion rate in this system is estimated to be $\dot{m} \sim 10^{-4}$ (Goodman & Lee 1989), which is low enough that thermalization at all radii is unlikely. Using an ADAF model with $\alpha = 0.3$ and $T_e \sim T_p(r/10^4)^{1/3}$ (§4.2) gives $r_{\text{th}}^e \sim 100$. For $r > 100$ the synchrotron spectrum would need to be calculated using the adiabatically compressed distribution function and would differ considerably from the spectrum calculated from a thermal distribution of electrons. Since lower frequencies in the synchrotron spectrum corresponds to emission from larger radii, the emission at frequencies $\sim 10^{10}$ Hz may be greatly reduced because of the new electron distribution function (cf. Fig. 3b). In particular, this may explain the extremely low radio flux of $\sim 10^{32}$ ergs s $^{-1}$ at $\nu \sim 10^{10}$ Hz (Crane et al. 1992) in M31, but detailed numerical calculations are required to confirm this hypothesis.

Another potential application of this work is in determining whether elliptical galaxies host dead quasars (Fabian & Canizares 1988). As suggested by Fabian & Rees (1995), ADAFs might allow elliptical galaxies to host $\gtrsim 10^8 M_\odot$ black holes and still remain dim. By varying the mass of the central black hole, Mahadevan (1997; see also Reynolds et al. 1996) has given spectra, which agree with the radio and X-ray upper limits, for a few of the nearby elliptical galaxies. He found that elliptical galaxies can host black holes up to $\lesssim 10^{9.5} M_\odot$, provided that they accrete via ADAFs. Interestingly, the constraint on the mass does not come from the X-ray data, but rather from the radio flux upper limit. Since these galaxies have estimated accretion rates (\dot{m}/α^2) $\lesssim 4 \times 10^{-4} M_8$ (Mahadevan 1997, eqn.[56]), where $M_8 = 10^8 M_\odot$, the radio spectrum may be reduced due to the adiabatically compressed electron distribution function. This would lead to a further increase in the allowed mass of the central black holes, therefore completely

eliminating the dead quasar host problem highlighted by Fabian & Canizares (1988).

A final application of this work is in determining accurate emission spectra from isolated black holes in the disk and halo of our Galaxy, which accrete from the interstellar medium. Ipser & Price (1982; 1977) have calculated spectra from these systems under the assumption that the black holes accrete by Bondi accretion and that the spectra is dominated by optically thin thermal synchrotron radiation. Even a small amount of angular momentum in the accreting gas precludes Bondi accretion, and so the gas is more likely to accrete onto the black hole as an ADAF. Furthermore, since these systems are likely to have low accretion rates ($\dot{m} \lesssim 10^{-5}$), the electrons are unable to thermalize and their distribution function is probably determined by adiabatic compression. The spectra from these systems will therefore be considerably different, with lower fluxes and luminosities peaking in different wave bands, than those obtained using a thermal distribution of electrons. Since the spectra from ADAFs are robust and well understood, detailed calculations of the spectra from isolated black holes, taking into account the non-thermal electron distribution function, would be quite valuable for the potential detection of these systems by the Sloan Digital Sky Survey. In addition, if no candidates are found, the ADAF spectrum will considerably modify the limits on halo black hole populations set by Heckler & Kolb (1996).

Acknowledgments. We thank Ramesh Narayan for many insightful and stimulating discussions throughout this work, and for comments on the manuscript. We also thank Ann Esin, Charles Gammie, Zoltán Haiman, Jeffrey McClintock, and George Rybicki for useful discussions. RM was supported by NSF grant AST 9423209 and EQ was supported by an NSF Graduate Research Fellowship.

A. Asymptotic Formulae for $I(x, n)$ and $I'(x, n)$

A.1. $I(x, n)$

The definition of $I(x, n)$ is given in equation (44):

$$I(x, n) \equiv \frac{1}{x} \int_0^\infty F\left[\frac{x}{z^2}\right] z^n \exp(-z^2) d\gamma. \quad (\text{A1})$$

This can be evaluated using the limiting forms for $F(x)$ (Rybicki & Lightman 1979; eqns. [6.34a,b]), which gives

$$\begin{aligned} I(x, 2) &\rightarrow \frac{2^{2/3}\pi}{\sqrt{3}} \frac{\Gamma(7/6)}{\Gamma(1/3)} x^{-2/3} = 1.01 x^{-2/3}, \quad x \ll 1, \\ I(x, 3) &\rightarrow \frac{2^{2/3}\pi}{\sqrt{3}} \frac{\Gamma(5/3)}{\Gamma(1/3)} x^{-2/3} = 0.98 x^{-2/3}, \quad x \ll 1, \end{aligned} \quad (\text{A2})$$

and

$$\begin{aligned} I(x, 2) &\rightarrow \frac{\pi}{2^{3/2}} x^{-1/4} \exp(-2x^{1/2}) = 1.11 x^{-1/4} \exp(-2x^{1/2}), \quad x \gg 1, \\ I(x, 3) &\rightarrow \frac{\pi}{2^{3/2}} \exp(-2x^{1/2}) = 1.11 \exp(-2x^{1/2}), \quad x \gg 1. \end{aligned} \quad (\text{A3})$$

A.2. $I'(x, n)$

The function $I'(x, n)$ is the angle averaged value of $I(x, n)$ and is defined by

$$I'(x, n) = \frac{1}{4\pi} \int I\left(\frac{x}{\sin \alpha_p}, n\right) d\Omega_p. \quad (\text{A4})$$

For $x \ll 1$ the integration is the same as done by Mahadevan et al. (1996), which gives

$$\begin{aligned} I'(x, 2) &\rightarrow \frac{2^{-1/3}\pi}{\sqrt{3}} \frac{\Gamma(7/6)\Gamma(1/2)}{\Gamma(11/6)} x^{-2/3} = 0.85 x^{-2/3}, \quad x \ll 1, \\ I'(x, 3) &\rightarrow \frac{2^{-1/3}\pi}{\sqrt{3}} \frac{\Gamma(5/3)\Gamma(1/2)}{\Gamma(11/6)} x^{-2/3} = 0.83 x^{-2/3}, \quad x \gg 1. \end{aligned} \quad (\text{A5})$$

For $x \gg 1$ we use the fact that most of the emission comes from $\sin \alpha_p \simeq 1$; the integrals can then be evaluated by a method similar to that given in Mahadevan et al. (1996). We obtain

$$\begin{aligned} I'(x, 2) &\rightarrow \frac{\pi^{3/2}}{4} x^{-1/2} \left(1 - \frac{1}{8x^{1/2}}\right) \exp(-2x^{1/2}) \simeq 1.39 x^{-1/4} \exp(-2x^{1/2}), \quad x \gg 1, \\ I'(x, 3) &\rightarrow \frac{\pi^{3/2}}{4} \exp(-2x^{1/2}) = 1.39 \exp(-2x^{1/2}), \quad x \gg 1. \end{aligned} \quad (\text{A6})$$

B. Compression factor in ADAFs

As discussed in §4.3, the quantity $p^3\rho^{-1}$ is conserved in the adiabatic compression of a monatomic ideal gas, which leads to the transformation $p \rightarrow ap \propto \rho^{1/3}p$ for the particle momenta. When the internal energy and pressure of the gas contain a contribution from the magnetic field, as in ADAF models, the form of the adiabatic invariant is more complicated. We make the *assumption* that the magnetic field always contributes a (constant) fraction β_{adv} of the total pressure and use this to determine the expression for the compression factor, a .

The gas pressure, P_g , and internal energy per unit mass, U_g , can be expressed in terms of an isotropic distribution function as

$$P_g = \frac{4\pi\rho}{3} \int dp \frac{n(p)p^4}{(p^2 + 1)^{1/2}} \quad (\text{B7})$$

and

$$U_g = 4\pi \int dp n(p)p^2 [(p^2 + 1)^{1/2} - 1] \equiv bP_g/\rho, \quad (\text{B8})$$

where, for simplicity, we set $m = c = 1$ in this Appendix. For the present purposes the distribution function is given by equation (38), that is,

$$n(p) = \frac{1}{(2\pi\tilde{a}^2)^{3/2}} \exp\left[\frac{-p^2}{2\tilde{a}}\right], \quad (\text{B9})$$

where $\tilde{a} \equiv a\sqrt{\theta_e}$. We treat this distribution function and the thermodynamic quantities U_g and P_g as functions of \tilde{a} and ρ . In this interpretation, the temperature (θ_e) which appears in the definition of \tilde{a} is a constant, namely the gas temperature when the adiabatic compression began.

For a gas in an isotropically tangled magnetic field, the total pressure is

$$P_{\text{tot}} = P_g + \frac{B^2}{24\pi} \equiv P_g/\beta_{\text{adv}} \quad (\text{B10})$$

and the total internal energy per unit mass is

$$U_{\text{tot}} = U_g + \frac{B^2}{8\pi\rho} = \frac{P_{\text{tot}}}{\rho} [3 + \beta_{\text{adv}}(b - 3)]. \quad (\text{B11})$$

Adiabaticity requires that $dU_{\text{tot}} = P_{\text{tot}}d\ln\rho/\rho$, which yields the following ordinary differential equation for the evolution of \tilde{a} as the gas is compressed.

$$\frac{d\ln\tilde{a}}{d\ln\rho} \left[(3 + \beta_{\text{adv}}(b - 3)) \frac{d\ln P_g}{d\ln\tilde{a}} + \beta_{\text{adv}} \frac{db}{d\ln\tilde{a}} \right] = 1. \quad (\text{B12})$$

In the non-relativistic limit, i.e., $\tilde{a} \ll 1$, $b = 3/2$, $db/d\ln\tilde{a} = 0$, and $d\ln P_g/d\ln\tilde{a} = 2$, which implies that $\tilde{a} \propto \rho^{1/(6-3\beta_{\text{adv}})}$. For equipartition magnetic fields, $\tilde{a} \propto \rho^{2/9} \propto r^{-1/3}$.

In the relativistic limit, $\tilde{a} \gg 1$, $b = 3$, $db/d\ln\tilde{a} = 0$, and $d\ln P_g/d\ln\tilde{a} = 1$; thus $\tilde{a} \propto \rho^{1/3} \propto r^{-1/2}$, independent of β_{rad} . We emphasize that in this context, relativistic vs. non-relativistic refers to the magnitude of \tilde{a} . It does not refer to the form of the distribution function, which is the same (eq. [B9]) regardless of the particle energies.

The above expressions for $\tilde{a}(\rho)$ in the non-relativistic and relativistic limits are precise analogs of the expressions for $T(\rho)$ for a thermal distribution given in §4.2. This is because the form of the distribution function (eq. [B9]) is only relevant when calculating the evolution of \tilde{a} through the non-relativistic/relativistic transition (which must be done numerically).

C. Departures from the Adiabatically Compressed Distribution Function

For a nearly thermal gas, the systematic and stochastic Fokker-Planck coefficients given in §3 yield the timescale on which a particle’s energy changes and thus the timescale on which the distribution becomes thermal. For non-thermal distribution functions, however, the distribution function may change on a timescale short compared to the thermalization timescale. As we now show, this implies that the adiabatically compressed distribution function given by equation (38) is only strictly valid for smaller \dot{m} than would be inferred from the thermalization timescales given in §3.

We consider only self-absorbed synchrotron radiation since it is more efficient than Coulomb collisions in modifying the distribution function. We also assume that, even for the non-thermal distribution function, the Fokker-Planck coefficients are given by (§3.2)

$$\frac{d\gamma}{dt} = C_1 B^2 \gamma^2 \left(1 - \frac{4\langle\gamma\rangle}{3\gamma} \right) \quad (\text{C13})$$

and

$$\frac{d(\Delta\gamma)^2}{dt} = 2C_1 B^2 \frac{\langle\gamma\rangle\gamma^2}{3}, \quad (\text{C14})$$

where we have replaced the temperature of the plasma with the average γ of the electrons, which is given by equation (39) for the adiabatically compressed distribution function.

The timescale on which the number of particles, $n(\gamma)$, at a given γ e-folds is given by $t_n \approx 1/|d\ln n(\gamma)/dt|$. This, not the systematic or diffusion timescales introduced in §3, is the relevant timescale when considering *departures from* a non-thermal distribution function (rather than *approaches to* a thermal distribution). Evaluating t_n for the adiabatically compressed distribution function, using the Fokker-Planck equation, yields (cf. eqs. [10], [38])

$$t_n = \frac{1}{C_1 B^2 \langle\gamma\rangle} \left| 8 - 4\frac{\gamma}{\langle\gamma\rangle} - \frac{104\gamma^2}{3\pi\langle\gamma\rangle^2} + \frac{8\gamma^3}{\pi\langle\gamma\rangle^3} + \frac{64\gamma^4}{3\pi^2\langle\gamma\rangle^4} \right|^{-1}, \quad (\text{C15})$$

where we have assumed that the electrons are relativistic. For large γ , the timescale on which the distribution function changes is $\sim (\gamma/\langle\gamma\rangle)^4$ times faster than the usual diffusion time, t_{diff}^s , and $\sim (\gamma/\langle\gamma\rangle)^3$ times faster than the usual systematic timescale, t_{sys}^s (eq. [23]). The physical reason for this is that diffusion can be much more efficient than is indicated by the stochastic Fokker-Planck coefficient if the non-thermal distribution function varies strongly with energy.

For accretion times less than the minimum of the diffusion and systematic timescales ($t_a < \min[t_{\text{diff}}^s, t_{\text{sys}}^s]$) it is incorrect to assume a thermal distribution function, but it is only if $t_a < t_n$ that it is strictly valid to assume that adiabatic compression yields the distribution function given by equation (38). This occurs provided that

$$\dot{m} \lesssim \frac{7.9 \times 10^{-5}}{\langle\gamma\rangle} r \alpha^2 \left(\frac{1 - \beta_{\text{adv}}}{0.5} \right)^{-1} \left| 8 - 4 \frac{\gamma}{\langle\gamma\rangle} - \frac{104\gamma^2}{3\pi\langle\gamma\rangle^2} + \frac{8\gamma^3}{\pi\langle\gamma\rangle^3} + \frac{64\gamma^4}{3\pi^2\langle\gamma\rangle^4} \right|^{-1} \quad (\text{C16})$$

For $\gamma \approx \langle\gamma\rangle$ there are no strong gradients in the distribution function and so the distribution function changes only on the energy diffusion time, i.e., $t_n \approx t_{\text{diff}}^s$. However, for $\gamma \approx 3\langle\gamma\rangle$, which is the Lorentz factor of the electrons responsible for most of the synchrotron emission, equation (C16) shows that the electrons have an adiabatically compressed distribution function only for accretion rates $\lesssim 10^{-6}\alpha^2 r$. This is a substantially more stringent requirement than the condition that thermalization be inefficient.

References

- Abramowicz, M., Chen, X., Kato, S., Lasota, J. P., & Regev, O., 1995, *ApJ*, 438, L37
- Abramowicz, M., Czerny, B., Laso, J. P., & Szuszkiewicz, 1988, *ApJ*, 332, 646
- Balbus, S. A., & Hawley, J.F. 1991, *ApJ*, 376, 214
- Crane, P. C., Dickel, J. R., & Cowan, J. J., 1992, *ApJ*, 390, L9-L12
- Dermer, C. D., & Liang, E. P., 1989, *ApJ*, 339, 512-528
- Esin, A., 1997, *ApJ*, 482, in press
- Fabian, A. C., & Canizares, C. R., 1988, *Nature*, 333, 829
- Fabian, A. C., & Rees, M. J., 1995, *MNRAS*, 277, L55-L58
- Frank, J., King, A., & Raine, D., 1992, *Accretion Power in Astrophysics* (Cambridge: Cambridge Univ. Press)
- Ghisellini, G., Guilbert, P. W., & Svensson, R., 1988, *ApJ*, 334, L5-L8
- Ghisellini, G., & Svensson, R., 1990, in *Physical Processes in Hot Cosmic Plasmas*, Vol. 305, ed. W. Brinkmann, A. C. Fabian, & F. Giovannelli (Dordrecht: Kluwer), 395
- Ghisellini, G., & Svensson, R., 1991, *MNRAS*, 252, 313-318
- Goodman, J., & Lee, H. M., 1989, *ApJ*, 337, 84-90
- Heckler, A. F., & Kolb, E. W., 1996, *ApJ*, 472, L85-L88
- Ipsier, J. R., & Price, R. H., 1977, *ApJ*, 216, 578-590
- Ipsier, J. R., & Price, R. H., 1982, *ApJ*, 255, 654-673
- Kormendy, J., & Richstone, D., 1995, *ARA&A*, 33, 581
- Landau, L. D., & Lifshitz, E. M., 1976, *Mechanics*, 3rd Ed., (Oxford: Pergamon Press)
- Lasota, J. P., Abramowicz, M. A., Chen, X., Krolik, J., Narayan, R., & Yi, I. 1996, *ApJ*, 462, 142
- Mahadevan, R., Narayan, R., & Yi, I., 1996, *ApJ*, 465, 327-337
- Mahadevan, R., 1997, *ApJ*, 477, 585-601
- Mahadevan, R., Narayan, R., & Krolik, J., 1997, *ApJ*, 486, in press
- McCray, R., 1969, *ApJ*, 156, 329-339
- Merck, M., et al., 1996, *A&A Sup.*, 120, 465-469
- Nakamura, K. E., Masaaki, K., Matsumoto, R., & Kato, S., 1997, *PASJ*, in press
- Narayan, R., & Yi, I., 1994, *ApJ*, 428, L13
- Narayan, R., & Yi, I., 1995a, *ApJ*, 444, 231
- Narayan, R., & Yi, I., 1995b, *ApJ*, 452, 710-735
- Narayan, R., Yi, I., & Mahadevan, R., 1995, *Nature*, 374, 623-625
- Narayan, R., 1996, *ApJ*, 462, 136
- Narayan, R., McClintock, J. E., & Yi, I., 1996, *ApJ*, 457, 821-833
- Narayan, R., Barret, D., & McClintock, 1997, *ApJ*, in press
- Narayan, R., Kato, S., Honma, F., 1997, *ApJ*, 476, 49-60
- Nayakshin, S., & Melia, F., 1997, *ApJ*, submitted, (astro-ph 9705011)
- Pacholczyk, A. G., 1970, *Radio Astrophysics* (San Francisco: Freeman)
- Rees, M. J., Begelman, M. C., Blandford, R. D., & Phinney, E. S., 1982, *Nature*, 295, 17
- Reynolds, C. S., Di Matteo, T., Fabian, A. C., Hwang, U., & Canizares, C. R., 1997, *MNRAS*, 1996, 283L, 111
- Rybicki, G., & Lightman, A., 1979, *Radiative Processes in Astrophysics* (New York: John Wiley & Sons, Inc.)
- Shakura, N. I., & Sunyaev, R. A., 1973, *A&A*, 24, 337
- Shapiro, S. L., Lightman, A. P., & Eardley, D. M. 1976, *ApJ*, 204, 187
- Spitzer, L. Jr., 1962, *Physics of Fully Ionized Gases*, 2nd Ed., (New York: John Wiley & Sons, Inc.)
- Stepney, S., & Gilbert, P.W. 1983, *MNRAS*, 204, 1269
- Trinchieri, G., Fabbiano, G., Canizares, C. R., 1986, *ApJ*, 310, 637-659

Figure Captions.

Figure 1: For accretion rates above a given curve in the figure, an electron with Lorentz factor γ is able to thermalize with a background plasma of temperature θ_e . The dashed lines represent thermalization through Coulomb collisions, while the solid lines represent thermalization through synchrotron self-absorption. The curves are determined by whether the dominant thermalizing process is systematic or diffusive acceleration (cf. eqs. [15], [25]). While thermalization by Coulomb collisions is, for a fixed temperature, independent of the radius r (cf. eq.[15]), the accretion rates required for thermalization by synchrotron self-absorption increase linearly with r (cf. eq. [25]).

Figure 2: a) A comparison of the momentum distribution function for a thermal gas of temperature $\theta_e \sim 1$ with that of an adiabatically compressed collisionless gas of the same energy. The adiabatically compressed gas is initially thermal and non-relativistic, but is then compressed to relativistic energies, resulting in a non-thermal distribution function. b) Analogous to a), but for the adiabatic expansion of a gas from relativistic to non-relativistic energies.

Figure 3: a) A comparison of the synchrotron radiation from a sphere of radius $\simeq 7 \times 10^{11}$ cm for an adiabatically compressed (solid line) and thermal (dashed line) gas with the same average energy. The electron number density and magnetic field strength are constant throughout the sphere ($n_e \simeq 10^{10} \text{ cm}^{-3}$ and $B \simeq 200$ Gauss). At low frequencies the radiation is highly self-absorbed, and the observed intensity is given by the source function, not the emissivity (dotted line) of the respective gases. b) The total synchrotron spectrum from an ADAF ($m = 2 \times 10^6$, $\dot{m} = 10^{-5}$) for adiabatically compressed electrons (solid line) and thermal electrons (dashed line) of the same average energy, which is assumed to be constant throughout the ADAF. This spectrum is obtained by summing the individual spectrum from each radius in the accretion flow, and thus accounts for the variation in electron number density and magnetic field strength with radius.

Figure 1

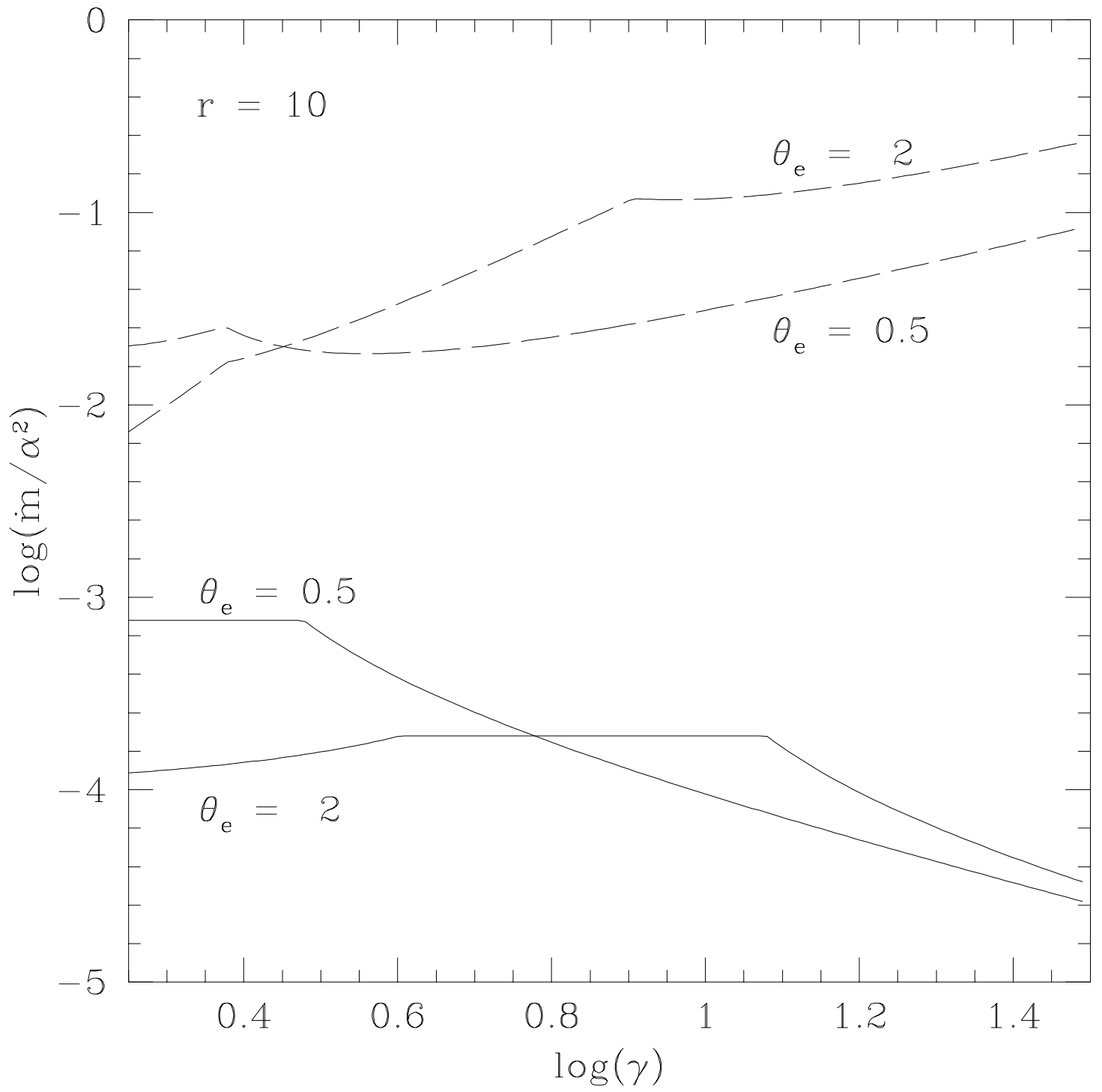


Figure 2

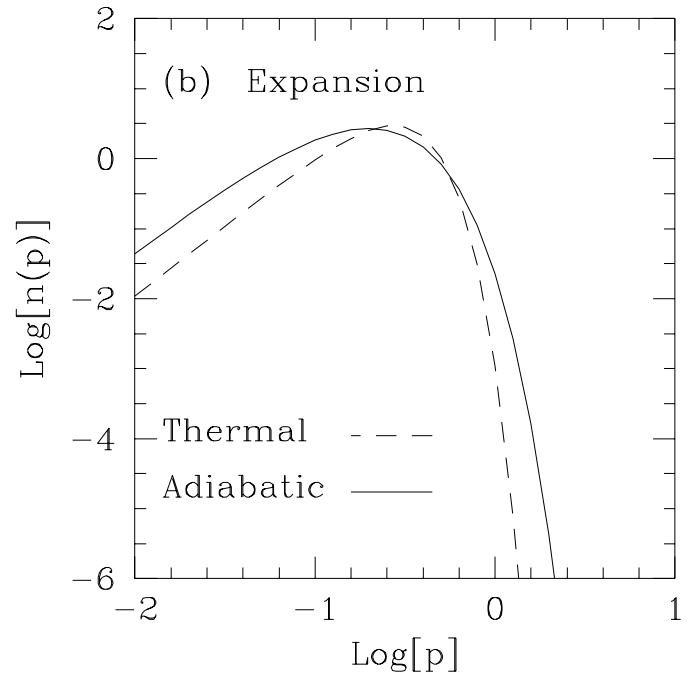
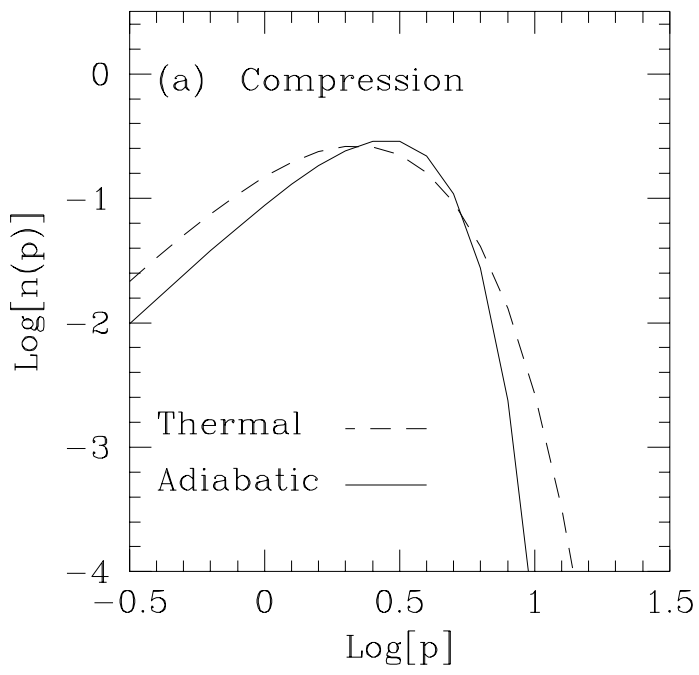


Figure 3

